Journal of Optoelectronics and Advanced Materials Vol. 6, No. 2, June 2004, p. 503 - 510

INVITED PAPER

ADVANCES IN AMORPHOUS AND NANOSTRUCTURED MATERIALS

R. Hasegawa*

Honeywell International, 440 Allied Drive, Conway, SC 29526 USA

Some of the emerging applications of amorphous magnetic materials are reviewed with emphasis on those utilizing the unique properties of these materials. In the area of nanostructured materials, recent advances made in understanding the basics of these materials are summarized, pointing out needed future research areas.

(Received April 26, 2004; accepted June 3, 2004)

Keywords: Amorphous materials, Nanostructured magnetic materials, Applications

1. Introduction

From a materials standpoint, amorphous magnetic alloys are slowly maturing in their development except in the areas in which specific applications are considered. In some of these cases, the first generation applications are becoming obsolete, followed by improvements or added features over the existing ones. One such example is the use of the magneto-mechanical resonance effect of amorphous alloys in electronic surveillance systems. The first generation material was based on an Fe-Ni-based alloy, followed by an Fe-Ni-Co-based alloy as outlined in Ref. 1. The new material exhibits improvement by a factor of two in the detection signal with an added feature of eliminating the problem of triggering other surveillance systems based on a different operating principle. The same material is also useful in other applications utilizing its unique magneto-elastic properties [2]. The change in the quality of electricity supply due to the ubiquitous use of electronic devices such as personal computers has increased the level of importance of using energy-saving amorphous metal-based electrical power transformers [3]. In future energy-generation efforts, attention is being directed to realize nuclear fusion plants based on heavy-ion acceleration devices utilizing amorphous or nanocrystalline materials [4]. New heat-treatments of the first generation Fe-based alloys have opened up opportunities for these alloys in applications in which more expensive Co-based amorphous alloys were used conventionally. Examples include sensors and band-pass filters [5]. Magnetic implements built from amorphous alloys in different forms, such as wire, powder, laminated sheets and bulk shapes, are on-going efforts [6].

While applications of nanocrystalline materials are not as wide as those of amorphous alloys, basic studies of these materials are quite active. In these efforts, an overall picture of nanostructure must incorporate chemical and topological short-range order as well as consideration of thermodynamic and magnetic driving force for atomic motion. Because of the multi-phases present in these materials, experimental methods to be utilized should be chosen accordingly. Especially needed are new techniques to monitor in-situ nanocrystallization processes in conjunction with the properties of post-nanocrystallization phases. These efforts will help develop new materials, leading to further advances in understanding the materials and their applications.

* Corresponding author: Ryusuke.Hasegawa@metglas.com

2. Amorphous materials

2.1. Energy-related applications

More data have been collected, showing impacts of harmonic distortions on transformer total losses in electrical power distribution systems. An example of the recent study in India is given in Table 1 as an illustration [7].

Table 1. Comparison of transformer losses of amorphous metal (AM) and grain-oriented silicon steel (Si-Fe)-based units. Total and linear losses are actual measured transformer loss and loss with no total harmonic distortion (THD), respectively.

A. Agricultural Site (three-phase 100 kVA units)

Core Material	Total Loss (W)	Linear Loss (W)	Loss Increase (W)	THD in Current (%)	THD in Voltage (%)
AM	700	679	21	3.5	2.6
Si-Fe	1300	710	590	2.3	1.4

B. Industrial Site (three-phase 250 kVA units)

Core Material	Total Loss (W)	Linear Loss (W)	Loss Increase (W)	THD in Current (%)	THD in Voltage (%)
AM	1726	1098	628	26	15
Si-Fe	2525	1550	975	26	15

The table above indicates that the frequency spectrum of the harmonic distortion is site-dependent since the load characteristic is different. In an industrial site, different industries use different power equipment, such as motor drives, which are known to introduce higher harmonic distortions. In an agricultural site, many units of a limited number of equipment, such as irrigation pumps, are used, thus the harmonic frequency spectrum has a small number of peaks resulting in a small number for THD. In any case, transformer loss increase due to THD in the power-line systems is considerably smaller in amorphous metal-based transformers than the conventional units. In most of the industrially developed countries, about one-half of the total electrical energy generated is used to run factories, transportation systems and office buildings where THDs are high in the energy distribution systems. Thus the impact of using amorphous metal-based units is significantly greater than has been thought.

As industrialization proceeds further in developing countries, the energy-saving aspect of amorphous metal-based transformers is becoming increasingly important. It is also becoming necessary to depend less on fossil fuel to generate electricity. In this area, amorphous and nanocrystalline magnetic materials have been considered most suited as shown in Ref. 4. The basic concept is the following: ion beams are accelerated in a linear particle accelerator through a succession of magnetic induction cores supplying a short- pulsed accelerating voltage for the beams which are confined in the core's axis direction. The ion beams are focused on a target of an ion fusion chamber. The heat produced from the fusion energy is converted to steam which then is utilized to generate electricity. It is estimated that a few $\times 10^7$ kg of magnetic core material is needed to drive such a fusion plant delivering several megajoules per pulse of energy to a target. Thus cost-effective core material is required, which provides particle accelerating pulse voltages efficiently.
Technically speaking, amorphous Fe-based alloys and Fe-based nanocrystalline alloys are desirable candidates for the core material, but the former materials provide the most economic solution at the present moment. The technical difference between the two classes of materials is that the nanocrystalline alloys exhibit lower magnetic loss for lower pulse magnetization rates than the amorphous alloys, while at higher magnetization rates both materials perform about the same [4]. Examples of the magnetic loss at a magnetization rate of 10^7 T/s are listed in Table 2 for the representative materials considered in Ref. 4. Since the acceleration voltage,V, in an induction core having a cross-section of S is generated following Faraday's law, a large flux swing ΔB within a short magnetization pulse duration Δt results in a large V ($=S\Delta B/\Delta t$). Thus, achieving high

magnetization rates ($\Delta B/\Delta t$) makes it possible to reduce core sizes. Therefore, these major factors must be considered in designing an efficient and cost-effective accelerator.

Table 2. Comparison of core loss for representative materials at a magnetization rate of 10^7 T/s. The thickness of the nanocrystalline and amorphous materials ranges between 16 and 21 μm.

(Data taken from Ref. 4.)

Material	Flux Swing ΔB (T)	Core Loss (J/m^3)
Fe-base nanocrystalline	2.1	1000
Amorphous Fe-B-Si-C	2.1	1200
Amorphous Fe-B-Si	2.1	1200
3% Si-Fe (25 μm thick)	3.0	5000

2.2. Sensors

Representative applications of amorphous alloys in sensors are summarized in Ref. 1-2.

New alloys have been recently reported for magnetic sensors including markers for electronic article surveillance (EAS) systems based on higher harmonic signal detection [8]. These alloys are based on Ni-Co-Fe and have relatively low saturation magnetostriction, λ_s, ranging from – 2 to + 2 ppm and saturation inductions, B_s, exceeding 0.5 T. A typical example is an alloy with a composition $Ni_{40}Co_{30}Fe_{10}(B, Si)_{20}$ having B_s= 0.58 T and λ_s= - 0.4 ppm. In Table 3, the harmonic signal level detected from this EAS marker is compared with a commercial one based on another Co-rich amorphous alloy.

Table 3. Comparison of harmonic signal response from $Ni_{40}Co_{30}Fe_{10}(B, Si)_{20}$ as-cast amorphous alloy and commercially available marker strips based on METGLAS®2705M with a length of 76 mm (data taken from Ref. 8). The fundamental frequency was 2.4 kHz and the detected signal was at its 25^{th} harmonics.

Alloy	Marker Width (mm)	Harmonic Response (mV)
Ni-Co-Fe-B-Si	3	240
METGLAS®2705M	3	150
Commercial 2705M Marker	2	160

It is noted that the harmonic signal response is increased significantly in the new alloy which contains less than one half of the cobalt in the commercially available METGLAS®2705M alloy. This will open up use of this alloy in other magnetic sensors.

2.3. New material synthesis

By electrodeposition, arrays of amorphous metal fine wire with diameters of 100-200 nm have been fabricated for Co-P and Ni-P systems [9, 10]. The coercivities of these wires are less than ~ 100 Oe, implying their low intrinsic magnetic anisotropies. Thus, if these wires are to be used in magnetic recording media, shape anisotropy must be utilized to compensate the magnetostatic interactions among the fine cylinders. The reduced remanence through the magnetostatic interaction and the low coercivity, however, are useful in micro-size magnetic components at high frequencies.

A two-step mechanical alloying has resulted in an amorphous Co-Fe-Zr powder with improved permeability in GHz region [11]. Compared with the conventional one-step process, the resultant powder is less agglomerated with a narrower size distribution after the second step using CCl_4 as the process control agent. The effects of the two step process seem to be composition-dependent and optimal for a $Co_{70}Fe_{20}Zr_{10}$ powder.

3. Nanostructured materials

3.1. Magnetic alloy development

A recent review on soft magnetic nanocrystalline alloys gives the following as a general chemical composition for these materials [12]:

$$\left(\begin{array}{l}\text{Fe}\\ \text{Co}\\ \text{Ni}\end{array}\right)_a \left(\begin{array}{lll}\text{Ti} & \text{V} & \text{Cr}\\ \text{Zr} & \text{Nb} & \text{Mo}\\ \text{Hf} & \text{Ta} & \text{W}\end{array}\right)_b \left(\begin{array}{lll}\text{B} & \text{C} & \\ \text{Al} & \text{Si} & \text{P}\\ \text{Ga} & \text{Ge} & \end{array}\right)_c \left(\begin{array}{l}\text{Cu}\\ \text{Ag}\\ \text{Au}\end{array}\right)_d$$

with a=60-90, b=2-8, c=8-31 and d=0-1 [13]. This formula allows us to explore possibilities for new alloys, which was the subject of this investigation. The case with Fe, Zr/Nb, B and Cu was reported in Ref. 12. The basic consideration in optimizing the magnetic properties of these alloys is (i) to increase their saturation inductions, and (ii) to reduce their magnetic anisotropies (K), saturation magnetostriction (λ_s), and exchange stiffness constants (A). The latter three factors are inter-related and therefore more difficult to optimize. In addition, the elements such as Ti in the second column affect compound formability upon nanocrystallization and the grain sizes of the resultant nanocrystals.

In contrast to the macroscopic view taken in the above case, more micro-scale adjustments result in improved hard magnets as reported in Ref. 14. For example, a high $(BH)_{max}$ product of 105 kJ/m^3 and intrinsic coercivity H_{ci} of 465 kA/m has been reported for a $Nd_{3.4}Dy_1Fe_{71.7}B_{18.5}Cr_{2.4}Co_{2.4}Cu_{0.4}Zr_{0.3}$ alloy with a remanence B_r of 0.97 T. Table 4 compares several hard magnets obtained through similar micro-scale adjustments and other nanostructured materials mentioned in this article together with the representative conventional materials. The reason for the necessity for the microscopic view in hard magnets is the following: the magnetic microstructure, which scales with $(A/K)^{1/2}$, essentially determines the level of Hci. The multi-component system mentioned above certainly provides the favorable microstructural condition needed. Clear evidence for a similar effect has been reported for a nano-clustered glassy Nd_{50} Fe_{40} Al_{10} alloy with a coercivity of 200-350 kA/m [15]. Without nano-clustering, the iso-compositional, random Nd_{50} Fe_{40} Al_{10} alloy shows a coercivity of about 100 kA/m. The nano-structure is characterized by exchange-coupled Fe-Nd clusters embedded in an Nd-rich amorphous matrix. This hard magnet has properties similar to those of a widely used Ba ferrite magnet as shown in Table 4. It is expected that these properties will be improved through further optimization of the chemical composition and fabrication process.

Table 4. Comparison of hard magnet properties of representative materials including commercially available magnets. The quantity $(BH)_{max}$, the maximum energy product, is a measure of performance as a permanent magnet. Currently $Nd_2Fe_{14}B$ magnet is the strongest hard magnet available.

Material (comp. in at.%) with [Ref]	B_r (T)	H_{ci} (kA/m)	$(BH)_{max}$ (kJ/m^3)
$Nd_{4.5}Fe_{73}B_{18.5}Cr_2Co_2$ [14]	1.05	378	108
$Nd_{3.4}Dy_1Fe_{72.3}B_{18.5}Cr_{2.4}Co_{2.4}$ [14]	0.98	398	87
$Nd_{3.4}Fe_{71.7}B_{18.5}Cr_{2.4}Co_{2.4}Cu_{0.4}Zr_{0.2}$ [14]	0.97	465	105
$Nd_{50}Fe_{40}Al_{10}$ [15]	0.40	200-350	~30
$Co_{80}Zr_{18}B_2$ [16]	0.43	400	38
Ba Ferrite	0.40	192	28
AlNiCo 5	1.20	58	40
Samarium-cobalt ($SmCo_2$)	0.90	696	160
Neodemium-iron-boron ($Nd_2Fe_{14}B$)	1.30	1120	320

Preferential nucleation/growth of a magnetically hard crystalline phase is one approach achieving a high-performance permanent magnet. An optimally annealed rapidly solidified Co-Zr-B

ribbon shows a $(BH)_{max}$ ~ 4.7 MGOe (see Table 4 above). The crystalline phase responsible for this is a metastable Co_5Zr [16].

3.2. Basic properties

Advances have been made to help us understand the relationship between the local structures and the observed properties of Fe-based nanocrystalline soft magnets. For example, their microstructures consisting of nanoparticles imbedded in amorphous matrices and their magnetic states have been well-characterized [17, 18]. However, the detailed processes leading to the microstructure formation are not well understood. Since the prototype precursor materials [17] contain a small amount (~1%) of Cu and it forms a clustering prior to the bcc Fe-Si nanocrystal formation, it has been argued that the clustered Cu atoms serve as the heterogeneous crystalline-nucleation centers. Some evidence for this has been reported [19]. However, a recent study shows that a bcc Fe-Co (Si) phase is formed prior to the Cu cluster formation in Fe-Co-Si-B-Nb-Cu alloys [20]. In addition, it has been known that Cu-free precursor alloys based on Fe-Zr-B result in nanocrystalline soft magnets [21]. It is, therefore, not necessary to have a small amount of Cu in the precursor systems. Its role is yet to be clarified, but the Cu clustering observed in 3D atom probe experiments [19, 20] is considered at the moment a by-product of a metallurgical process in which the system rejects Cu atoms in the process of forming a bcc crystalline phase in an amorphous matrix. This is not inconsistent with the observation that the Cu clustering takes place adjacent to the bcc nanocrystals.

The efforts thus far adopted to clarify the nanocrystalline formation are through semi-static kinetic processes such as thermal annealing. Thus its dynamic nature has not been studied extensively. In this sense, recent studies on the crystallization behaviors in amorphous alloys under electron-irradiation [22] and electropulsing [23] are instructive.

The driving forces for the atomic motion by these techniques are supplied by an elastic energy transfer during electron-irradiation or enhanced electromigration through collective motion of atoms. Since these processes take place at or below room temperature, kinetics involved in conventional thermal annealing are minimized. What matters in these processes is the structural stability of the area targeted, and the resultant crystallization follows, to a first degree, through polymorphous transformations. Thus, chemical and topological short-range orders for the constituent atoms in the precursor amorphous alloys play a major role in nanocrystallizaton, being consistent with the observations thus far made. Therefore the non-thermal processes mentioned above would shed more light if they were utilized in conjunction with the conventional thermal annealing as implied in Ref. 22.

The 3D atom probe mentioned above provides local structural and chemical compositions and is a powerful tool for studying the nanocrystalline states. Its magnetic counterpart is the Mössbauer spectroscopy in which different magnetic phases with different chemical and topological short-range orders centered around Fe atoms can be separately probed [24]. Thus snap shots during amorphous-to-crystalline transformation can be monitored [25]. Detailed studies along this line of work show the following [24-26]. There exist three different short-range environments for Fe atoms: a bcc Fe in the nanocrystals, an amorphous Fe-based phase and a disordered Fe-rich interface between bcc Fe and the amorphous matrix. These phases have been clearly identified as shown in Fig. 1 taken from Ref. 24 which contains a number of other similar cases. Ref. 26 is an extension of this work and clarifies the significance of the interface region. A schematic representation of the atomic arrangement is given in Fig. 2 of Ref. 26. Thus the magnetic interactions among the three phases have become clearer, helping for example, molecular-field type analysis and simulation to become more refined. The three magnetic phases have different Curie temperatures which are desired to be as high as possible from application standpoints. Studying a material with these features at elevated temperatures, however, is accompanied by complications due to materials' propensity toward crystallization. To avoid this, Cr, which tends to increase crystallization temperatures and reduce Curie temperatures, has been added to the Fe-based alloys [27]. This has made the magnetic phenomena more readily accessible temperature-wise without uncertainties arising from the possible structural changes.

As exemplified in the above, local spectroscopic techniques provide pertinent information on the fine atomic arrangements in the nanostructured materials. However, the observations are stroboscopic; more dynamic time-dependent techniques would be of help in understanding the evolution of the atomic motion during nanocrystallization by thermal processes. For example, a widely used DSC becomes a more useful tool if combined with other types of similar techniques such as resistivity measurement as shown in Fig. 2 which is taken from Ref. 28. A DSC scan is normally taken at a given heating rate and as such it probes a time-dependent thermal process. Resistivity, on the other hand, depends on electron scattering which is a much shorter process than the thermal process, providing a unique supporting information for a disordered material in which electron mean-free path is of the order of the interatomic distance. The results obtained through these approaches would become instructive if compared with those through non-thermal processes [22, 23] mentioned above.

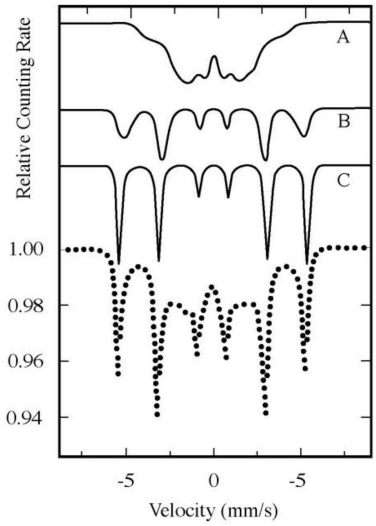

Fig. 1. A transmission Mössbauer spectrum (bottom curve) taken at room temperature on a nanocrystalline $Fe_{80}Ti_7Cu_1B_{12}$ alloy annealed at 470 ^oC for one hour. The curves A, B and C correspond to the spectrum components from the amorphous Fe-based matrix, Fe-rich interface region and the bcc Fe-based nanocrystalline grains, respectively. Data taken from Ref. 24.

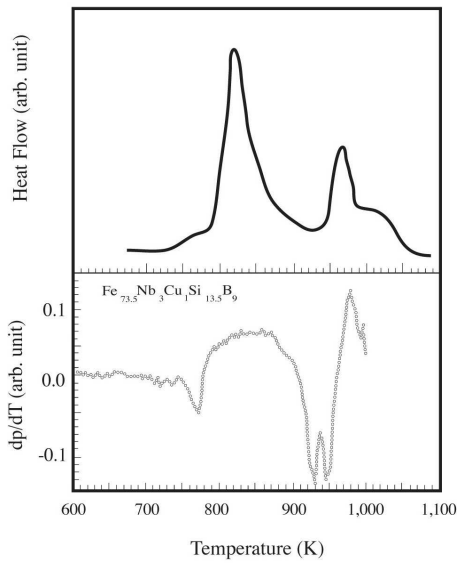

Fig. 2. DSC scan (upper figure) and temperature dependence of $d\rho/dT$ where ρ is the resistivity of a nanocrystallline $Fe_{73.5}Nb_3Cu_1Si_{13.5}B_9$ (data taken from Ref. 28).

3.3. Applications

A number of soft magnetic applications of nanocrystalline magnetic materials have been considered and are commercially available. These include common-mode electrical chokes, high frequency transformers, pulse-power cores, magnetic sensors, magnetic shielding sheets and the like. Development of Fe-Co based alloys [29] is expected to lead to magnetic devices operated at high temperatures. This work is to evolve to micro-structural investigations of the constituent phases interacting magnetically and structurally among themselves and search for new device opportunities which do not exist currently due to materials' performance limitations.
Controlled fabrication is necessary for applications of low-dimensional nanostructured materials such as fine fibers and nanosize particles. The future of MEMs, micromagnetic components and medical use of these materials [30] depends on how these materials evolve.

4. Conclusion

Energy-related applications of amorphous magnetic materials are becoming increasingly relevant and therefore will grow in size. The material development side of this field is more application-specific and the vast amount of technical information accumulated thus far has helped develop new materials effectively and timely. Nanocrystalline materials, on the other hand, are structurally more complex, but the basic understanding of these materials is progressing well. New insights into direct observation of the dynamic nanocrystallization processes are necessary for further progress.

References

[1] R. Hasegawa, U.S. Patent No. 5, 628, 840 (1997).
[2] R. Hasegawa, J. Non-Cryst. Solids, **287**, 405 (2001).
[3] R. Hasegawa, D. C. Pruess, Proceedings of IEEE Power Engineering Society Summer Meeting (July 2001, Vancouver, Canada).
[4] A. W. Molvik, A. Faltens, Phys. Rev. Special Topics-Accelerators and Beams, **5**, 080401 (2002).
[5] R. Hasegawa, Proceedings of NATO Advanced Research Workshop "Prosize" (Budmerice, Slovakia, June 2003), to be published.
[6] R. Hasegawa, J. Non-Cryst. Solids, **329**, 1 (2003).
[7] U. C. Trivedi, V. Gupta and R. Hasegawa, Proceedings of International Power Engineering Conf. (September 2003, Singapore).
[8] R. Hasegawa, H. H. Liebermann, R. J. Martis, U.S. Patent No. 6, 475,303 (2002).
[9] M. Shima, M. Hwang, C. A. Ross, J. Appl. Phys, **93**, 3440 (2003).
[10] H. Chiriac, N. Lupu, Proceedings of NATO Advanced Research Workshop "Prosize" (June 2003, Budmerice, Slovakia), to be published.
[11] L. W. Deng, J. J. Jiang, S. C. Fan, Z. K. Feng, W. Y. Xie, X. C. Zhang, H. H. He, J. Mag. Mag. Materials **264**, 50 (2003).
[12] K. Suzuki, Proceedings of NATO Advanced Research Workshop "Prosize" (June 2003, Budmerice, Slovakia), to be published.
[13] The ranges for a, b, c and d are slightly different than those given in Ref. 12.
[14] K. Hono, D. H. Ping, T. Ohkubo, M. Ohnuma, Proceedings of NATO Advanced Research Workshop "Prosize" (June 2003, Budmerice, Slovakia), to be published.
[15] N. Lupu, H. Chiriac, Proceedings of NATO Advanced Research Workshop "Prosize" (June 2003, Budmerice, Slovakia), to be published.
[16] T. Saito, Appl. Phys. Lett. **82**, 2305 (2003).
[17] Y. Yoshizawa, S. Oguma, K. Yamauchi, J. Appl. Phys. **64**, 6044 (1988).
[18] G. Herzer, IEEE Trans. Magn. **25**, 3327 (1989).

[19] K. Hono, D. H. Ping, M. Ohnuma, H. Onodera, Acta Mater. **47**, 997 (1999).
[20] M. Ohnuma, D. H. Ping, T. Abe, H. Onodera, K. Hono, Y. Yoshizawa, J. Appl. Phys. **93**, 9186 (2003).
[21] K. Suzuki, N. Kataoka, A. Inoue, A. Makino, T. Masumoto, Mater. Trans. JIM **31**, 743 (1990).
[22] T. Nagase, Y. Umakoshi, Mat. Sci. & Eng. **A347**, 136 (2003).
[23] H. Mizubayashi, T. Hao, H. Tanimoto, J. Non-Cryst. Solids, **312-314**, 581 (2002).
[24] M. Miglierini, J.-M. Greneche, J. Phys.: Condens. Matter **9**, 2303 (1997).
[25] M. Miglierini, I. Tóth, M. Seberíni, E. Illeková, B. Idzikowski, J. Phys.: Condens. Matter **14**, 1249 (2002).
[26] J. M. Greneche, A. Ślawska-Waniewska, J. Mag. Mag. Materials **215-216**, 264 (2000).
[27] V. Franco, L. F. Kiss, T. Kemény, I. Vincze, C. F. Conde, A. Conde, Phys. Rev. **B66**, 224418 (2002).
[28] J. M. Barandiarán, Proceedings of NATO Advanced Research Workshop "Prosize" (June 2003, Budmerice, Slovakia), to be published.
[29] M. A. Willard, D. E. Laughlin, M. E. McHenry, D. Thoma, K. Sickafus, J. O. Cross, V. G. Harris, J. Appl. Phys. **84**, 6773 (1998).
[30] Q. A. Pankhurst, J. Connolly, S. K. Jones, J. Dobson, J. Phys. D: Appl. Phys. **36**, R167 (2003).